Published in final edited form as:

Cell Rep. 2024 March 26; 43(3): 113822. doi:10.1016/j.celrep.2024.113822.

Hair cell regeneration, reinnervation, and restoration of hearing thresholds in the avian hearing organ

Mitsuo P. Sato[1,2,3], **Nesrine Benkafadar**[1,2], **Stefan Heller**[1,2,4,*]

[1]Department of Otolaryngology-Head and Neck Surgery, Stanford University School of Medicine, Stanford, CA 94305, USA

[2]Institute for Stem Cell Biology and Regenerative Medicine, Stanford University School of Medicine, Stanford, CA 94305, USA

[3]Department of Otolaryngology-Head and Neck Surgery, Kindai University School of Medicine, Osaka, Japan

[4]Lead contact

SUMMARY

Hearing starts, at the cellular level, with mechanoelectrical transduction by sensory hair cells. Sound information is then transmitted via afferent synaptic connections with auditory neurons. Frequency information is encoded by the location of hair cells along the cochlear duct. Loss of hair cells, synapses, or auditory neurons leads to permanent hearing loss in mammals. Birds, in contrast, regenerate auditory hair cells and functionally recover from hearing loss. Here, we characterized regeneration and reinnervation in sisomicin-deafened chickens and found that afferent neurons contact regenerated hair cells at the tips of basal projections. In contrast to development, synaptic specializations are established at these locations distant from the hair cells' bodies. The protrusions then contracted as regenerated hair cells matured and became functional 2 weeks post-deafening. We found that auditory thresholds recovered after 4–5 weeks. We interpret the regeneration-specific synaptic reestablishment as a location-preserving process that might be needed to maintain tonotopic fidelity.

Graphical abstract

*Correspondence: hellers@stanford.edu.

AUTHOR CONTRIBUTIONS

Conceptualization, M.P.S., N.B., and S.H.; methodology, M.P.S. and N.B.; formal analysis, M.P.S.; investigation, M.P.S. and N.B.; visualization, M.P.S.; funding acquisition, M.P.S., N.B., and S.H.; project administration, S.H.; supervision, N.B. and S.H.; writing – original draft, M.P.S. and N.B.; writing – review & editing, M.P.S., N.B., and S.H.

SUPPLEMENTAL INFORMATION

Supplemental information can be found online at https://doi.org/10.1016/j.celrep.2024.113822.

DECLARATION OF INTERESTS

The authors declare no competing interests.

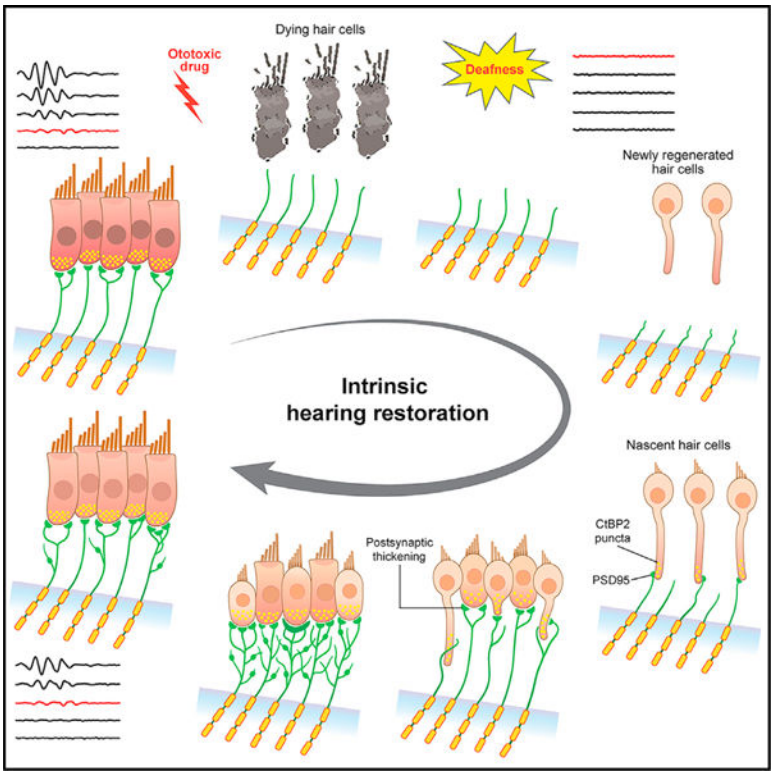

In brief

Sato et al. provide a timetable of the cytomorphological maturation and reinnervation of newly regenerated avian auditory hair cells, leading to functional recovery of hearing thresholds. Synapse reformation happens via an unusual mechanism at the tips of hair cell projections that reach toward afferent neurites near the basement membrane.

INTRODUCTION

Sensory cells in the cochlea, known as hair cells, are essential for auditory perception. Hair cells are compact cylindrical cells that convert mechanical stimuli of their apical hair bundle into the release of synaptic vesicles at afferent synapses with the dendrites of auditory neurons. The auditory neurons relay the sound-encoding post-synaptic potentials and generate action potentials. These electrical signals are transmitted along the axons of the auditory nerve, carrying them toward the brainstem, where central auditory processing starts.

Every component of the peripheral auditory system is crucial for our ability to perceive sound. Hair cells, synapses, and afferent neurons are susceptible to damage from various sources, including loud noises, specific medications, and the inevitable consequences of aging.[1] This vulnerability results in hearing loss. Mammals lack the inherent capacity to regenerate lost cochlear hair cells or effectively repair damaged synaptic connections, resulting in incurable hearing impairment.

Non-mammalian vertebrates, unlike mammals, can replace auditory hair cells throughout life. Age-related hearing loss, for example, does not exist in starling species.[2] Chickens can readily recover from drug- and noise-induced hair cell loss,[3] and songbirds can relearn vocal mimicry after recovery from deafness.[4,5] At the core of the avian ability to naturally recover from hearing loss are facultative stem cells that, upon injury, divide and replace lost hair cells.[6–8] These facultative stem cells are also called supporting cells; it remains a mystery why mammalian supporting cells have lost their ability to regenerate lost hair cells.[9]

The avian equivalent of the mammalian cochlea, the basilar papilla, has been used as an attractive model to study hair cell regeneration for decades.[10–12] Damage methods that use systemic administration of ototoxic drugs such as aminoglycosides or acoustic trauma often affect only the base to middle regions of the basilar papilla.[13–16] Systemic ototoxic drug administration can lead to nephropathy and morbidity, while acoustic trauma can have a variable impact on the morphology of surviving hair cells[17,18]; high-level sound exposure can cause supporting cell loss.[19] Moreover, systemic aminoglycoside injection can result in the shrinkage of afferent and efferent nerve terminals on surviving hair cells, while acoustic trauma destroys efferent nerve endings.[13,19] This variability can be reduced with carefully titrated systemic aminoglycoside-based damage models.[20]

We hypothesized that surgical delivery of the chemically well-defined ototoxin sisomicin directly into the chicken inner ear would further reduce variability,[21] and we utilized a single infusion of the ototoxic drug sisomicin that elicits complete hair cell loss at 24 h post-sisomicin treatment (PST).[22] This injury triggers a highly synchronized regenerative response of supporting cells that, combined with single-cell transcriptomic profiling, allows us to unravel signaling pathways that activate the regenerative capacity of supporting cells *in vivo*.[23,24] Because birds do functionally recover from hearing loss and are able to restore auditory synapses and afferent innervation,[13–16] we hypothesized that an animal model with complete hair cell loss and a synchronized regenerative response would allow us to investigate the time course of afferent reinnervation of newly regenerated hair cells and the functional restoration of auditory function.

To interrogate the reconnection of newly regenerated hair cells with auditory neurons, we focused on the avian tall hair cells, which correspond to mammalian inner hair cells and are mainly innervated by afferent fibers.[25–27] Tall hair cells are located medially in a cross-section of the avian hearing organ (Figure 1A). Here, we present a time course of functional restoration that begins with the retraction of neurites, followed by the reconnection of afferent fibers with newly regenerated tall hair cells. We identified a process in which the new hair cells exhibit protrusions that extend toward the basement membrane of the sensory epithelium, where the first new pre- and post-synaptic specializations are established. Reinnervation and morphological hair cell maturation subsequently manifest in a dynamic retraction of the hair cells' protrusions, ultimately resulting in the typical cylindrical hair cell morphology and the restoration of synapses. This regenerative activity is distinct from the innervation process of avian hair cells during embryonic development, highlighting its specialized nature. Functional recovery, based on hearing threshold restoration, starts 9 days PST, and reaches pre-damage levels within 28 to 35 days. Our findings illustrate

the exceptional regenerative potential of the avian hearing organ and provide a mechanistic template for mammalian auditory restoration.

RESULTS

Time course of basilar papilla hair cell regeneration

Immunohistochemistry at various time points PST revealed a consistent time course of hair cell regeneration in the chicken's basilar papilla (Figures 1A–1H). One day after sisomicin infusion into the lateral semicircular canal, we observed complete extrusion of all auditory hair cells (Figure 1B). The extruded dead hair cells remained detectable using antibodies to Myosin 7A (MYO7A) and displayed F-actin-containing cellular debris as well as fragmented nuclear material 1 day PST (Figure 1B; Figure S1B). Dead hair cell debris lacked the typical cylindrical morphologies and distinct hair bundle shapes seen in undamaged controls (Figure 1A; Figure S1A). This rapid elimination of all basilar papilla hair cells and preservation of the supporting cells is consistent with previous findings.[22] Release of dead hair cells into the *scala media* has also been reported in mice.[28] New hair cells were first detected with MYO7A immunostaining at 5 days PST. They were predominantly located in the medial side of the sensory epithelium (Figure 1C), indicating that tall hair cells reappear before short hair cells, which we first detected 7 days PST (Figure 1D). Immature-appearing short hair bundles were apparent at 7 days PST, and the number of newly regenerated hair cells increased over the next 2 weeks (Figures 1E and 1F). Over time, hair cell regeneration and maturation continued, resulting in a typical cytomorphological appearance of hair cells along the whole basilar papilla between 21 and 35 days PST (Figures 1F–1H; Figures S1C–S1F). MYO7A-immunoreactivity of hair cell debris remained detectable in the *scala media* through all time points of our investigation (Figures 1C–1H; Figure S1B). Quantitative analysis revealed no significant difference in tall and short hair cell numbers at 3–5 weeks PST compared to control, while tall hair cell regeneration preceded short hair cell reemergence (Figure 1I). From 3 weeks PST onwards, the regenerated hair cells displayed mature morphology. Hair bundles were not detected in newly generated hair cells at day 5 PST, were clearly visible with F-actin staining at day 7 PST, and maturated over time; their heights and widths were equal to controls at 11 days PST (Figures 1J–1L).

Neurite retraction following sisomicin-induced hair cell loss

To assess the effects of sisomicin infusion and hair cell loss on auditory ganglion afferent neurites, we performed immunolabeling with beta III tubulin (TUBB3) antibodies. One day PST, after hair cell extrusion, we observed neurite retraction and sparser TUBB3 labeling within the sensory epithelia compared to the control (Figures 2A–2D). All afferent neurites along the medial-lateral axis, and the whole length of the basilar papilla rescinded toward the superior fibrocartilaginous plate (Figures 2B–2D). Efferent nerve fibers innervating the hyaline cells were also immunolabeled for TUBB3 and remained unaffected (Figures 2B–2H, arrowheads in 2B), suggesting that the afferent neurite retraction was in response to the loss of hair cell targets and not a general neurotoxic effect of sisomicin on nerve fibers. The neurites appeared unaffected at 12 h PST when the hair cells were still intact (Figure 2E). Over the course of the first 4 days PST, the neurites remained withdrawn from the damaged

sensory epithelium (Figures 2F and 2G), principally remaining in a holding pattern near the basement membrane at 4 days PST (Figure 2H).

To ascertain that sisomicin infusion had no toxic effect on neurons, we conducted TUNEL assays. Twenty hours PST, hair cell nuclei were TUNEL positive (Figure S2A), indicating apoptotic hair cell death, which is the expected result of the sisomicin treatment.[22] We did not detect TUNEL-positive supporting cells, glial cells, or ganglion cells at 20 h or 2 and 3 days PST (Figure S2A), suggesting the viability of these cell groups. The number of auditory ganglion cells remained constant during the neurite retraction phase (Figures S2B and S2C). Based on these findings, we conclude that sisomicin infusion does not induce apoptosis of auditory ganglion or glial cells.

Reinnervation

Regrowth of retracted neurites coincided with the emergence of the newly regenerated hair cells (Figures 2I–2K). Nascent hair cells, in contrast to mature hair cells, can be immunolabeled with anti-TUBB3 antibodies and display elongated cytomorphology with discernable TUBB3- and MYO7A-positive basal protrusions toward the basement membrane (Figures 2L–2N). This fact limits the use of TUBB3 for tracking the reinnervation of newly regenerated hair cells. We, therefore, used antibodies to neurofilament (NF200) to label afferent neurites and to distinguish TUBB3-positive neurites from TUBB3-positive basal hair cell projections, which allowed us to track neurites over time (Figure 3A). At 5 days PST, the neurites remained retracted near the basement membrane. Extension of NF200-positive neurites and contact with basal hair cell protrusions were first observed at 7 days PST (Figure 3A). As hair cell maturation progressed, neurite outgrowth continued, and some neurites formed post-synaptic-like thickenings that were noticeable at 9 days PST (Figure 3A, 9 days: inset and arrowheads). As reinnervation proceeded, cup-like contacts of neurites with new hair cells became more numerous and were initially quite large (Figure 3A, 14 days, arrow) but became smaller at 21 days PST and refined to mainly two per hair cell at 28 days PST, which is comparable to the undamaged control (Figure 3B). We refer to these cup-like contacts as pre-synaptic thickenings, which have been anatomically described to be associated with 2–3 afferent nerve fibers per tall hair cell in various avian species.[25,29] Antibodies to TUBB3 strongly labeled the pre-synaptic thickenings, which were also associated with the post-synaptic density protein 95 (PSD95), which retains AMPA-type glutamate receptors at the post-synapse (Figure S3A, control). PSD95 labeling reemerged after 4 days and was associated with TUBB3-positive afferent neurite endings (Figure S3A).

Although the pronounced TUBB3-positive projections that extend from newly regenerated hair cells from day 5 PST onwards (Figure 3A, 5–9 days) are not labeled with anti-NF200 antibodies, we wanted to ensure that they are hair cell protrusions. Monoclonal antibodies to otoferlin exquisitely label avian hair cells[30] and allowed us to clarify further the relationship between the hair cell protrusions and neurites. Hair cells in control specimen showed strong otoferlin immunoreactivity (Figure 3C). Newly formed hair cells at day 5 PST were weakly expressing otoferlin, but their basal projections displayed robust otoferlin immunoreactivity (Figures 3C and 3C′). Moreover, the otoferlin-positive tips were associated with the NF200-

labeled afferent neurites (Figures 3C′ and C″), as well as with PSD95-labeled post-synaptic thickenings (Figure S3B). As reinnervation progressed, the protrusions immunolabeled with otoferlin antibody retracted toward the hair cells' bodies and became shorter and thicker.

New hair cells lost TUBB3 immunoreactivity from PST day 14 onwards and no longer expressed TUBB3 at day 28. Based on our immunohistochemical assessment, we conclude that reinnervation was nearly complete at 4 weeks PST (Figures 3A and 3B), extended along the whole tonotopic axis (Figures S4A–S4C), and appeared fully mature at 5 weeks PST (Figures S4D–S4F).

Reformation of synaptic structures

During the formation of auditory circuits, the synaptic activity of maturing hair cells is essential for proper development and maturation.[31] We hypothesized that the appearance of the pre-synaptic marker C-terminal binding protein 2 (CTBP2) would indicate the early essential stages of this process. CTBP2 is typically associated with distinct pre-synaptic punctae at the base of tall hair cells in the basilar papilla (Figure 4A, control). The first CTBP2-positive dots were observed at 6 days PST at the tips of the basal projections of newly regenerated hair cells, indicating that pre-synaptic structures first emerge basally and distant from the new hair cells' bodies (Figure 4A, 6 days). The punctae were gradually detected more apically, coinciding with the retraction of the hair cell projections. When the hair cells acquired their typical cylindrical morphology at 14 days PST, the CTBP2-positive punctae settled at the regular basal location below the nucleus.

Next, we used an antibody to PSD95 to examine whether post-synaptic structures correlate with pre-synaptic specializations during reinnervation. In control hair cells, PSD95 immunolabeling is detected in the post-synaptic thickenings at the terminals of afferent neurites (Figure 4B; Figure S3A). PSD95 immunoreactivity disappeared after hair cell loss and reappeared at the tips of afferent neurites after day 4 PST (Figure S3A). At day 6 PST, close to CTBP2-positive dots in hair cell projections, we also detected PSD95-positive neurite tips near the basement membrane (Figure 4B). This correlation was robust and persisted throughout the reinnervation process. PSD95-labeled post-synaptic thickenings were associated with the migration of CTBP2 punctae and were detected at their regular basal location at 14 days PST.

We quantified the number of CTBP2-positive punctae over time PST compared to undamaged controls (Figure 4C). At 6 days PST, about half of the typical number of punctae were found. These punctae were located, on average, at a distance of 29 μm basally from the bottom of the hair cells' nuclei (Figures 4D and 4E). The number of CTBP2-positive dots increased from PST day 6 until day 11, and, simultaneously, the average distance of the dots from the hair cells' nuclei decreased. At 11 days PST, the number of CTBP2-positive dots was not significantly different from controls, and the dots were not significantly distant from the hair cells' nuclei compared to controls. Together, our findings indicate that pre- and post-synaptic specializations form early during new hair cell maturation at the tips of basal hair cell protrusions and at the tips of afferent neurites. Hair cells and neurites appear to interact at these sites akin to the two index fingers in Michelangelo's fresco painting *Creazione di Adamo*.[32] The CTBP2-positive punctae subsequently migrate apically together

with the contracting basal protrusions; this process coincides with afferent neurite extension. The most dynamic phase of this process happens between PST days 7 and 11. The process, in general, was obvious and abundantly noticeable in the medial (neural) region of the basilar papilla. In the lateral region, mainly innervated by efferent nerves, basal projections were also obvious, and CTBP2-positive punctae were found, albeit less abundantly, at the tips of short hair cell protrusions (Figure S3C).

A potential role for calretinin during functional basilar papilla restoration

Calretinin, an EF-hand Ca^{2+}-binding protein encoded by *CALB2*, is crucial in modulating Ca^{2+} influx and regulating exocytosis in sensory hair cells.[33] Previous studies have demonstrated the expression of calretinin in inner and outer hair cells as well as in auditory neurons during the development of the mouse cochlea, with no detectable expression in supporting cells.[34] A recent single-cell transcriptome study found CALB2 expression in the regenerating basilar papilla supporting cells and nascent regenerated hair cells.[24] To investigate the potential involvement of calretinin during functional basilar papilla restoration, we performed immunohistochemistry following sisomicin infusion. In control sections, calretinin was not detectable in hair cells; occasional but inconsistent dotted labeling was identified basolaterally near synapses (Figure 5A).

At 5 days PST, we observed robust calretinin expression in the nuclei of supporting cells and in new hair cells (Figure 5B). Over time, we noticed that calretinin expression was first lower in supporting cell nuclei of the medial region of the basilar papilla at 7 days PST (Figure 5C). Calretinin immunoreactivity gradually shifted toward the lateral side at 14 days PST, when the protein was detected in the cytoplasm of new short hair cells and in the nuclei of supporting cells; calretinin expression in new tall hair cells was markedly lower (Figure 5D). This progression continued through 21 days PST until 28 days PST, when calretinin expression was sparse but still detectable mainly in the lateral region (Figures 5E and 5F).

We quantified calretinin expression in each cell type in the medial and lateral regions over time (Figure 5H). Notably, calretinin expression was observed in supporting cells' nuclei before the newly regenerated hair cells emerged (Figures 5G and 5H). The expression of the calcium buffer protein declined earlier on the medial/neural side, with supporting cells exhibiting a more rapid decrease compared to hair cells (Figure 5H). Albeit correlative, we note that the downregulation of calretinin expression in new tall hair cells and in supporting cells of the medial region coincided with the most dynamic phase of hair cell protrusion condensation and neurite extension (Figure 5I). These observations suggest a potential role for calretinin and increased mobile Ca^{2+} buffer capacity in the regenerative processes associated with new hair cell maturation and the reestablishment of sensory function in the basilar papilla.

Comparison of regeneration and development

Our observation that newly regenerated hair cells exhibit basal projections that establish interactions with the retracted neurites is reminiscent of pre-synaptic projections of zebrafish lateral line hair cells during neural circuitry formation.[35] This raised the question of whether the afferent innervation of newly differentiated hair cells in the avian basilar papilla

generally happens through short-range projections. Goodyear and colleagues reported otoferlin-rich hair cell processes in the embryonic day (E) 7–8 basilar papilla,[30] suggesting that basal projections are a hallmark of newly generated hair cells. To investigate similarities and differences between regeneration and development, we examined how basilar papilla hair cells are innervated during embryonic development.

The first hair cells were detectable with antibodies to TUBB3 in the developing basilar papilla as early as E6.5. The nascent hair cells featured basal protrusions similar to the newly differentiated hair cells during regeneration (Figure 6A). Concurrently, NF200 immunostaining revealed the extension of neurites into the sensory epithelium toward the hair cells (Figure 6B). Expression of MYO7A was first detected in developing short hair cells at E7 and appeared in the medial tall hair cells at E8. Putative post-synaptic condensations at the basal poles of developing hair cells were first observed at E8. During the refinement process, the neurites displayed buds and large synaptic thickenings (Figures 6A and 6B). In contrast to regenerated hair cells, we found that CTBP2 expression during the development of hair cells exclusively occurred below the nuclei and not at the tips of the basal protrusions, starting at E8–E8.5 (Figure 6C). This suggests that nascent hair cells, during development, project toward the afferent neurites, which is similar to new hair cells during regeneration. However, pre-synaptic specializations during development are established subnuclearly at the basal poles.

Furthermore, the transient expression of calretinin during hair cell development was restricted to hair cells and, similar to regeneration, ceased first in tall hair cells at E16 (Figure 6D). In contrast to regeneration, we did not detect calretinin expression in supporting cells during hair cell specification, but some expression was noticeable in lateral supporting cells at E16.

Functional recovery

We conducted auditory brainstem response (ABR) measurements in sisomicin-infused chickens to evaluate hearing restoration during basilar papilla regeneration. Because cross-hearing from the unaffected ear can alter the responses of interest in animals with one-sided deafness,[36] it was necessary to prevent inputs from the untreated ear. We refrained from bilateral sisomicin infusion because preservation of vestibular function of the unaffected side is essential to avoid gait disturbance and malnutrition caused by bilateral vestibular dysfunction. Therefore, we selectively removed the basilar papilla on the unaffected side without damaging the vestibule. We confirmed that the extraction of the basilar papilla on the unaffected side did not significantly alter the ABRs of the opposite side (Figures S5A and S5B).

We measured ABRs in sisomicin-infused chickens before and at various time points PST (Figure 7A). First, we attempted to identify the time point of initial hearing recovery. The chickens lacked detectable ABR thresholds at 3 days PST (Figure 7B). Although deafness persisted until 7 days PST with no detectable thresholds, we detected high thresholds at 9 days PST (Figure 7B). Modest threshold recovery was first consistently detected at 11 days PST, coinciding with our observation of the time courses of hair bundle formation, as well as the initiation of reinnervation and synaptic reformation (Figures 1, 3, and 4). We conclude

that the first physiologically detectable auditory recovery happens between 9 and 11 days PST. This finding supports the conclusion that new hair cells have mechanoreception and functional synapses during their cytomorphological maturation, probably becoming more mature with the conclusion of basal projection contraction.

Next, we examined hearing restoration from 11 days PST onwards. Over time, the hearing thresholds gradually recovered, eventually converging to an average threshold deficit of 6.3–18.5 dB, which was principally not significantly different from pre-infusion and age-matched controls (Figures 7B and 7C; Figure S5C). We found some variability of functional recovery, with some animals reaching pre-infusion hearing thresholds and others having an up to 20 dB shift at 5 weeks PST (Figure S5D). We presume that 5 weeks PST represents the earliest time point when complete functional recovery can be expected, and based on the visible trend of recovery over time (Figure 7B), we conclude that auditory restoration in completely deafened chickens is highly efficient and can reach pre-damage levels. This remarkable regenerative capability of the avian inner ear stands in stark contrast to the complete regenerative inertness of the mammalian cochlea.

DISCUSSION

Ototoxic drug administration is a suitable strategy for investigating inner ear regeneration in avian models and is generally less variable compared to acoustic trauma.[5,17] We directly applied sisomicin to the inner ear, which induces complete loss of auditory hair cells within the first 24 h PST.[22,24] This method avoids the nephrotoxicity, variability, and protracted damage responses observed with systemic aminoglycoside treatments.

Previous reports, mainly in mice, showed a reciprocal dependence of hair cells and auditory ganglion neurons where dysfunction in one cell type can affect the survival of the other cell type.[37–41] It is important to note that despite the reported reliance on trophic factors released by murine hair cells, auditory ganglion neurons usually do not degenerate quickly. Moreover, this dependence seems less relevant in humans, where auditory neurons can survive for decades without their hair cell targets and become functionally integrated again in cochlear implant patients. This is an important consideration because future regenerative treatments in humans will require surviving auditory ganglion neurons. In our study, we were motivated by this perspective to investigate the interrelationship of hair cell loss and newly regenerated hair cells with their innervating auditory ganglion cells in chickens. Because avians functionally restore hearing after hair cell loss, we presumed that the reinnervation of newly regenerated hair cells is a well-orchestrated process.

Our experiments were designed based on the previously determined time course of hair cell demise and proliferative hair cell regeneration in the chicken basilar papilla after semicircular canal infusion of sisomicin.[22,24] Using the same hair cell loss paradigm, we characterized hair cell loss, regeneration, reestablishment of afferent innervation, and functional auditory recovery in the chicken.

Tropic dependence of auditory ganglion neurons has been reported in developing chickens.[42] Forced activation of Wnt signaling showed that ectopic sensory patches were innervated,

suggesting that hair cells attract neurites during embryonic development.[43] Several studies have put forward specific factors released from hair cells as attractants of afferent nerves during innervation in the development of chicken and mouse ears.[44,45] In this context, BDNF, among other guidance molecules, has been shown to be crucial for innervation.[46] Although the sensory epithelia do not require afferent innervation for differentiation,[41] a close interaction between hair cells and auditory neurons has been suggested to coordinate mutual maturation.[47–49]

In our study, we found that nascent auditory hair cells display basal projections toward the afferent neurites. These projections appear to be a hallmark of newly differentiated hair cells in development as well as during regeneration. We noted, however, that the location of the emerging synapse differs between development and regeneration. In development, CTBP2-positive punctae, indicators of the forming pre-synapse, were first detectable right below the hair cells' nuclei, which is more or less the same location as synapses in mature hair cells. The synapses, therefore, are assembled at the basal poles of developing hair cells and not at the tips of the hair cells' basal protrusions. In contrast, newly regenerated hair cells established synaptic connections far away from the cells' nuclei at the tips of their basal projections. As the projections shortened over the course of several days, the contacting neurites followed and grew toward the hair cell bodies, where the location and number of synaptic connections were reestablished.

We interpret that the regenerated hair cells "reaching down" toward the afferent neurites might reflect an omission of non-specific long-range neurite attractants normally present during development. Furthermore, this reaching process might be needed to preserve the tonotopic organization of the regenerating basilar papilla. We suggest that establishing direct local contact points suppresses the sprouting of neurites. The system, therefore, prevents the formation of synaptic contacts with hair cells that do not already match the established frequency-specific central projections of the auditory neurons. In conclusion, we propose that the observed mechanism of reinnervation of newly regenerated hair cells in the chicken auditory epithelium is specialized to preserve tonotopy. This preservation is not required during development because central projections are not mature. It is interesting in this context that basal hair cell protrusions were also found during zebrafish neuromast development but the locations of the emerging synapses were the same as in adults.[35] Neuromasts are part of the lateral line system for detecting water currents and providing spatial orientation. Hair cells in the neuromast are organized into two opposing groups that define the organ's axis of best sensitivity to water flows. We surmise that tonotopy preservation is irrelevant in neuromasts and that afferent reinnervation, therefore, differs from the avian auditory system. In mammals, basal projections have not been reported except in the mature vestibular system, where vestibular hair cells display processes that appear to form synapses with the vestibular afferent nerve several cell diameters away.[50] Additional work is needed to determine the mechanism by which basal hair cell projections and afferent neurites find each other. Existing single-cell datasets from newly regenerated avian auditory hair cells exist,[24] but additional datasets from auditory neurons obtained post-damage are needed for in-depth analyses of candidate genes.

Newly differentiated immature hair cells express high levels of CALB2, encoding the mobile intracellular Ca^{2+} buffer calretinin. Calretinin expression in regenerated tall hair cells on the medial side of the basilar papilla overlapped with the establishment of afferent innervation and ceased upon functional recovery, based on ABR measurements. We can only speculate about the role of calretinin and mobile Ca^{2+} buffers during regeneration. Ca^{2+} signaling is important for hair cell function and regulates cellular projections.[33,51] High levels of calretinin and Ca^{2+} signaling per se might be involved in the formation and retraction of hair cell protrusions during the reestablishment of afferent connections. Moreover, high calretinin levels might also modulate synaptic activity during reinnervation. The enrichment of otoferlin at the tips of newly regenerated hair cells' basal projections is another indication of a possible role for Ca^{2+} that is based on otoferlin's role in Ca^{2+}-triggered neurotransmitter release from mammalian auditory hair cells.[52,53]

To ensure a comprehensive and systematic comparison, we conducted a thorough analysis of the morphological characteristics of hair cells at various embryonic stages, aiming to establish correlations with the regenerative process. By closely examining the similarities and differences between regeneration and development, our primary objective was to gain insights into the specific mechanisms governing hair cell regeneration.

Our findings provide compelling evidence that the morphological changes observed during hair cell regeneration bear striking resemblances to developmental processes. Our study revealed the formation of neurite branches and buds during reinnervation. Additionally, we observed swelling of afferent nerve endings and pronounced post-synaptic density formation. Previous research has indicated that these phenomena occur during inner ear development in chickens and mice.[54,55] Furthermore, it has previously been shown that regenerating hair cells exhibited functional features shared with developing hair cells, such as the presence of Ca^{2+} channels necessary for spontaneous action potentials that could contribute to the survival and refinement of neuronal connections.[56] The different location of emerging pre-synaptic specializations was the most striking difference between developing hair cells and regenerated hair cells. As already laid out, we speculate that this difference is owed to a different environment during regeneration where preservation of tonotopy is critical.

The investigation of functional recovery following inner ear damage has been an area of focus since the discovery of hair cell regeneration in chickens after acoustic trauma.[6] ABR thresholds returned to almost normal within 30–70 days after discontinuing systemic aminoglycoside administration except for the high frequencies.[5,10] Persistent hearing loss at high frequencies was suggested to result from the cumulative effects of multiple traumas,[15,57] while faster recovery at low-mid frequencies might be attributed to insufficient damage in the mid-apex regions. In a study involving local gentamicin administration with collagen sponges placed at the round window of the pigeon cochlea, complete hair cell loss, except for 20% of the apex, and maximum hearing loss were observed 5–7 days after treatment.[58] Hearing loss at all frequencies showed minimal improvement until 13 days, followed by gradual recovery over time, resulting in hearing threshold shifts averaging 7–28 dB after approximately 70 days. However, their findings also indicated a sluggish improvement in hearing thresholds around 28 days after treatment. It should be noted that

while these functional recovery results align with our study, structural recovery, including reinnervation, was not analyzed, and the prolonged effects of gentamicin sponges could have affected the outcomes. To comprehensively track hearing restoration accompanied by regenerated basilar papilla, ABR measurements should be coupled with evaluations of reinnervation, synaptic reformation, and regenerated hair cell maturation.

We found that regeneration starts already during hair cell demise, leading to supporting cell activation.[23] Tall hair cell regeneration commences through a mainly proliferative mechanism[24] and features afferent neurite retraction, a dynamic interplay between new hair cells' basal projections and neurite reinnervation, accompanied by synaptic reformation. Functional recovery is indicated by the improvement of ABR thresholds over time and also reflects the time course of functional recovery of afferent innervation.

Overall, our study provides valuable insights into the remarkable regenerative capacity and functional recovery of the avian hearing organ. The gradual functional recovery observed in our study emphasizes that the regenerative process comprises multiple interconnected stages. This insight will contribute to future studies on hair cell regeneration and the development of potential therapeutic interventions for hearing loss.

Limitations of the study

While the study focused on hair cell regeneration and functional recovery, it did not extensively explore the broader auditory system, including central auditory processing and connectivity between regenerated hair cells and higher auditory centers. A deeper investigation into these aspects would provide a more holistic understanding of the regenerative process. In addition, we focused on afferent reinnervation of tall hair cells that happens primarily in the medial region of the basilar papilla. We show that short hair cells regenerate in our animal model and that hearing threshold recovery is nearly complete 5 weeks post-damage. Such a recovery can only happen with functional short hair cells integrated into the efferent feedback loop that regulates cochlear amplification. However, we did not explicitly show the recovery of the amplification process and the efferent reinnervation of short hair cells. The latter requires additional markers and tools that need to be established for the avian model. Lastly, the specific mechanisms underlying hair cell regeneration, such as candidate genes for neurite outgrowth and synapse formation, as well as the functional role of calretinin, were not fully elucidated. Future research should delve into the molecular pathways and signaling mechanisms involved in hair cell regeneration and reinnervation to identify potential therapeutic targets for hearing loss treatment.

STAR★METHODS

RESOURCE AVAILABILITY

Lead contact—Further information and requests for resources and reagents should be directed to and will be fulfilled by the lead contact, Stefan Heller (hellers@stanford.edu).

Materials availability—The study did not generate new unique reagents.

Data and code availability

- All data reported in this paper will be shared by the lead contact upon request.
- No original code was developed.
- Any additional information required to reanalyze the data reported in this paper is available from the lead contact upon request.

EXPERIMENTAL MODEL AND STUDY PARTICIPANT DETAILS

All animal care and procedures complied with the Guide for the Care and Use of Laboratory Animals published by the National Institutes of Health. Fertilized pathogen-free chicken eggs were purchased from Charles River Laboratories. Chicken hatching, housing, and animal procedures were approved by the Stanford University Institutional Animal Care and Use Committee and performed as described.[22]

We took all necessary steps to minimize animal suffering, including the use of anesthesia and analgesia during surgical procedures, and careful monitoring of animal health and welfare. Both male and female animals were included in all analyses.

METHOD DETAILS

Animals for experiments—Fertilized chicken eggs (Charles River, Wilmington, USA) were used for the experiments. The eggs were placed in a humidified incubator set to 39°C with continuous egg rocking for 19 days and then transferred to a Brinsea Octagon incubator for hatching. The hatchlings were moved to a brooder cage equipped with an infrared heat lamp, digital thermometer, chick starter feed, and water. The chickens were raised in a calm and quiet environment with a 12-h artificial day-night cycle.

Infusion via the semicircular canal—On post-hatch day 7, chickens were anesthetized by administering 3% isoflurane and 2 L/min oxygen using a nose cone. The anesthetized chickens were positioned on a heating pad in the right lateral recumbent position. Anesthesia was maintained by delivering 2% isoflurane and 2 L/min oxygen. Subcutaneous injection of carprofen at 1 mg/kg was administered near the breast under the wing. Feather removal in the postauricular area was performed using Nair, followed by three alternating treatments with diluted betadine and 70% isopropanol. A 6–7 mm incision was made in the skin to expose the temporal bone's surface. The lateral semicircular canals' bony labyrinth was punctured using a 30 ½-gauge needle, resulting in slight discharge of perilymph. Infusion into the semicircular canal was carried out using a Micropump (UMP3Micro 4, World Precision Instruments) and a 35-gauge blunt Nanofil needle (World Precision Instruments) at a rate of 8 nL/s, delivering 2 μL sisomicin solution at 75 μg/μL in phosphate-buffered saline at pH 7.4 (PBS). The puncture wound was sealed with bone wax (Ethicon), and the skin wound was closed using surgical superglue. To facilitate the emergence from anesthesia, pure oxygen was provided, and the chicken was transferred onto bedding into a small plastic container. The chicken was closely monitored for 15 min before returning to the cage. Each chicken was identified with colored leg bands (Chicken Hill) for individual labeling purposes.

Dissection of the chicken basilar papilla and vibratome sectioning—Following euthanasia by CO_2 inhalation and subsequent decapitation, the chicken heads were bisected, and the temporal bone containing the basilar papilla was carefully excised using surgical scissors. The excised temporal bone was then placed in a solution of 4% paraformaldehyde in PBS and incubated overnight at 4°C. For developmental studies, eggs were candled to confirm viability, gently cracked open using surgical scissors, and the embryo was transferred to a Petri dish filled with PBS. The entire head was excised, immersed in 4% paraformaldehyde in PBS, and incubated overnight at 4°C. After rinsing the excised tissue with PBS, the basilar papillae were dissected and embedded in disposable molds containing liquid 4% low melt agarose in PBS. The embedded basilar papillae were positioned appropriately for cutting and stored in a humidified chamber at 4°C. Transverse sections of the basilar papillae were obtained using a Leica VT1200 vibratome with parameters set to 60–70 mm thickness, 1mm amplitude, and a cutting speed of 0.7 mm/s. The resulting sections were punched out using a 1.5 mm biopsy punch on a Sylgard 184 silicone plate. Additional details of this method are available.[59]

Immunohistochemistry—Immunostaining procedures were generally performed as previously described.[22] We used the following antibodies: rabbit polyclonal antibodies to MYO7A, NF200, PSD95, CALB2, and mouse monoclonal antibodies to SOX2, TUBB3, and CTBP2. For visualization, donkey anti-mouse and anti-rabbit IgG secondary antibodies conjugated to Alexa 488 or Alexa 546 were employed. F-ACTIN was visualized using phalloidin conjugated with Alexa 647, and nuclei were identified using DAPI. For the PSD95 antibody, we adopted a different method, using a blocking buffer containing 3% BSA and 1% donkey serum in PBS, followed by permeabilization with 3% Triton in PBS, and culminating in a 36–40 h incubation with the primary antibody at 4°C. The DeadEnd fluorometric TUNEL System was used to detect apoptotic DNA fragmentation. After staining, the sections were mounted on glass slides using an antifade medium with a 0.12 mm spacer between the slide and coverslip. All experiments were performed at least in triplicate, and representative images are presented.

Auditory brainstem response—The auditory brainstem response measurements were conducted according to a previously published protocol.[60] Chickens were positioned in a prone position with a beak rest while under general anesthesia induced by an anesthetic cocktail comprising Ketamine (50 mg/kg) and Xylazine (16.7 mg/kg). If the animals started to regain consciousness and exhibited movement during the experiment, an additional injection of half the original dosage was administered. Three stainless steel needle electrodes were subdermally inserted at specific sites: the active electrode positioned above the midline of the skull, the reference electrode placed below the ear canal of interest, and the ground electrode positioned on the dorsal side of the neck. Prior to each ABR recording session, sound level calibration was carried out, and electrode impedance was confirmed to be below 1.0 kΩ. Body temperature was maintained at 39°C using a heating pad throughout the testing process. Tone burst stimuli were used within a frequency range of 64–5600 Hz, with a rise/fall time of 1 ms and a duration of 10 ms. The stimulus count was set at 1024 sweeps, and the presentation rate was maintained at 10–20 stimuli per second. The signal was filtered with a low pass of 100 Hz and a high pass of 3000 Hz. The sound stimuli were initially

decreased in 10-dB steps and subsequently in 5-dB steps until the hearing threshold was determined. ABR measurements were conducted both before and after sisomicin infusion at various time points. To avoid cross-hearing, the unaffected ear was deafened by extracting the columella through a hole of the tympanic membrane followed by removal of the basilar papilla through the oval window. This procedure, which did not involve any skin incision and resulted in minimal bleeding, lasted approximately 5 min

QUANTIFICATION AND STATISTICAL ANALYSIS

Statistical significance was evaluated using one-way ANOVA for the hair bundle height and width, the number of ganglion cells, and the number and distance of CTBP2-positive punctae. CTBP2-positive punctae were counted in 5 adjacent hair cells per sample in volumes of $60 \times 60 \times 60$ mm^3. We used Imaris imaging software to unequivocally identify individual hair cells in 3-dimensional space. In hair cell protrusions, we ensured that we count punctae associated with a single protrusion that can be traced back to a single hair cell. In general, we found that hair cells displayed only single protrusions. The distance between CTBP2-positive punctae and regenerated hair cell nuclei was determined by measuring the lines from the point of contact of the tangential line against the nuclei to associated CTBP2-positive dots. Regarding counting the number of hair cells, the boundary between tall and short hair cells was first determined using age- and location-matched control samples. After calculating the percentage of each area of the total cross-section's width, we defined the medial/tall hair cells' and the lateral/short hair cells' locations; the boundary, defined as 10% of the total width, was removed to avoid equivocal counts. Only sections that were perpendicular to the longitudinal axis were considered. Then, each MYO7A-positive hair cell with more than half a visible nucleus was counted in the 80 μm deep volume, represented by 40 individual optical sections. Hair cell numbers were assessed with a two-way ANOVA followed by Dunnett's multiple comparison test to compare experimental and control data. For the analysis of ABR data, Tukey's multiple comparisons test was employed. All statistical tests were performed using GraphPad Prism 8 software.

Supplementary Material

Refer to Web version on PubMed Central for supplementary material.

ACKNOWLEDGMENTS

We want to express our sincere gratitude to members of the Heller laboratory for their valuable discussions and critical review of the manuscript. We also thank the OHNS microscopy core facility for their expert assistance with imaging and Chris Gralapp for illustrations (chrisgralapp.com). M.P.S. acknowledges support from the Soda Toyoji SPIO Scholarship 2022 (no. SS22002). N.B. received support from the School of Medicine Dean's Postdoctoral Fellowship, the American Hearing Research Foundation, and the Katharine McCormick Advanced Postdoctoral Scholar Fellowship, which provides support for women in academic medicine. For their support, we thank the Hearing Restoration Project Consortium of the Hearing Health Foundation, the Stanford Initiative to Cure Hearing Loss, and the National Institutes of Health grant R01-DC019619 (S.H.).

REFERENCES

1. Wagner EL, and Shin JB (2019). Mechanisms of Hair Cell Damage and Repair. Trends Neurosci 42, 414–424. 10.1016/j.tins.2019.03.006. [PubMed: 30992136]

2. Langemann U, Hamann I, and Friebe A (1999). A behavioral test of presbycusis in the bird auditory system. Hear. Res 137, 68–76. [PubMed: 10545635]

3. Rubel EW, Furrer SA, and Stone JS (2013). A brief history of hair cell regeneration research and speculations on the future. Hear. Res 297, 42–51. 10.1016/j.heares.2012.12.014. [PubMed: 23321648]

4. Dooling RJ, Ryals BM, and Manabe K (1997). Recovery of hearing and vocal behavior after hair-cell regeneration. Proc. Natl. Acad. Sci. USA 94, 14206–14210. 10.1073/pnas.94.25.14206. [PubMed: 9391178]

5. Ryals BM, Dent ML, and Dooling RJ (2013). Return of function after hair cell regeneration. Hear. Res 297, 113–120. 10.1016/j.heares.2012.11.019. [PubMed: 23202051]

6. Corwin JT, and Cotanche DA (1988). Regeneration of sensory hair cells after acoustic trauma. Science 240, 1772–1774. 10.1126/science.3381100. [PubMed: 3381100]

7. Ryals BM, and Rubel EW (1988). Hair cell regeneration after acoustic trauma in adult Coturnix quail. Science 240, 1774–1776. 10.1126/science.3381101. [PubMed: 3381101]

8. Janesick AS, and Heller S (2019). Stem Cells and the Bird Cochlea-Where Is Everybody? Cold Spring Harb. Perspect. Med 9, a033183. 10.1101/cshperspect.a033183. [PubMed: 30249599]

9. Brigande JV, and Heller S (2009). Quo vadis, hair cell regeneration? Nat. Neurosci 12, 679–685. 10.1038/nn.2311. [PubMed: 19471265]

10. Smolders JW (1999). Functional recovery in the avian ear after hair cell regeneration. Audiol. Neurootol 4, 286–302. [PubMed: 10516389]

11. Stone JS, and Cotanche DA (2007). Hair cell regeneration in the avian auditory epithelium. Int. J. Dev. Biol 51, 633–647. [PubMed: 17891722]

12. Saunders JC (2010). The role of hair cell regeneration in an avian model of inner ear injury and repair from acoustic trauma. ILAR J 51, 326–337. [PubMed: 21131710]

13. Duckert LG, and Rubel EW (1990). Ultrastructural observations on regenerating hair cells in the chick basilar papilla. Hear. Res 48, 161–182. 10.1016/0378-5955(90)90206-5. [PubMed: 2249958]

14. Duckert LG, and Rubel EW (1993). Morphological correlates of functional recovery in the chicken inner ear after gentamycin treatment. J. Comp. Neurol 331, 75–96. 10.1002/cne.903310105. [PubMed: 8320349]

15. Cotanche DA, Lee KH, Stone JS, and Picard DA (1994). Hair cell regeneration in the bird cochlea following noise damage or ototoxic drug damage. Anat. Embryol 189, 1–18.

16. Wang Y, and Raphael Y (1996). Re-innervation patterns of chick auditory sensory epithelium after acoustic overstimulation. Hear. Res 97, 11–18. [PubMed: 8844182]

17. Saunders JC, Adler HJ, and Pugliano FA (1992). The structural and functional aspects of hair cell regeneration in the chick as a result of exposure to intense sound. Exp. Neurol 115, 13–17. [PubMed: 1728559]

18. Umemoto M, Sakagami M, Fukazawa K, Ashida K, Kubo T, Senda T, and Yoneda Y (1995). Hair cell regeneration in the chick inner ear following acoustic trauma: ultrastructural and immunohistochemical studies. Cell Tissue Res 281, 435–443. 10.1007/BF00417861. [PubMed: 7553765]

19. Ofsie MS, and Cotanche DA (1996). Distribution of nerve fibers in the basilar papilla of normal and sound-damaged chick cochleae. J. Comp. Neurol 370, 281–294. [PubMed: 8799856]

20. Cafaro J, Lee GS, and Stone JS (2007). Atoh1 expression defines activated progenitors and differentiating hair cells during avian hair cell regeneration. Dev. Dynam 236, 156–170. 10.1002/dvdy.21023.

21. Janesick A, Scheibinger M, and Heller S (2022). Molecular Tools to Study Regeneration of the Avian Cochlea and Utricle. Developmental, Physiological, and Functional Neurobiology of the Inner Ear 176, 77–97. 10.1007/978-1-0716-2022-9_5.

22. Benkafadar N, Janesick A, Scheibinger M, Ling AH, Jan TA, and Heller S (2021). Transcriptomic characterization of dying hair cells in the avian cochlea. Cell Rep 34, 108902. 10.1016/j.celrep.2021.108902. [PubMed: 33761357]

23. Benkafadar N, Sato MP, Ling AH, Janesick A, Scheibinger M, Jan TA, and Heller S (2024). An essential signaling cascade for avian auditory hair cell regeneration. Dev. Cell 59, 280–291.e5. 10.1016/j.devcel.2023.11.028. [PubMed: 38128539]

24. Janesick AS, Scheibinger M, Benkafadar N, Kirti S, and Heller S (2022). Avian auditory hair cell regeneration is accompanied by JAK/STAT-dependent expression of immune-related genes in supporting cells. Development 149, dev200113. 10.1242/dev.200113. [PubMed: 35420675]
25. Fischer FP (1998). Hair cell morphology and innervation in the basilar papilla of the emu (Dromaius novaehollandiae). Hear. Res 121, 112–124. 10.1016/s0378-5955(98)00072-0. [PubMed: 9682814]
26. Gleich O, and Manley GA (2000). The Hearing Organ of Birds and Crocodilia. In Comparative Hearing: Birds and Reptiles (Springer). 10.1007/978-1-4612-1182-2_3.
27. Janesick A, Scheibinger M, Benkafadar N, Kirti S, Ellwanger DC, and Heller S (2021). Cell-type identity of the avian cochlea. Cell Rep 34, 108900. 10.1016/j.celrep.2021.108900. [PubMed: 33761346]
28. Taylor RR, Nevill G, and Forge A (2008). Rapid hair cell loss: a mouse model for cochlear lesions. J. Assoc. Res. Otolaryngol 9, 44–64. 10.1007/s10162-007-0105-8. [PubMed: 18057986]
29. Fischer FP, Miltz C, Singer I, and Manley GA (1992). Morphological gradients in the starling basilar papilla. J. Morphol 213, 225–240. 10.1002/jmor.1052130207. [PubMed: 29865594]
30. Goodyear RJ, Legan PK, Christiansen JR, Xia B, Korchagina J, Gale JE, Warchol ME, Corwin JT, and Richardson GP (2010). Identification of the hair cell soma-1 antigen, HCS-1, as otoferlin. J. Assoc. Res. Otolaryngol 11, 573–586. 10.1007/s10162-010-0231-6. [PubMed: 20809368]
31. Tritsch NX, Rodríguez-Contreras A, Crins TTH, Wang HC, Borst JGG, and Bergles DE (2010). Calcium action potentials in hair cells pattern auditory neuron activity before hearing onset. Nat. Neurosci 13, 1050–1052. 10.1038/nn.2604. [PubMed: 20676105]
32. Michelangelo (c. 1512). Creazione di Adamo Sistine Chapel, Vatican City.
33. Pangršič T, Gabrielaitis M, Michanski S, Schwaller B, Wolf F, Strenzke N, and Moser T (2015). EF-hand protein Ca2+ buffers regulate Ca2+ influx and exocytosis in sensory hair cells. Proc. Natl. Acad. Sci. USA 112, E1028–E1037. 10.1073/pnas.1416424112. [PubMed: 25691754]
34. Dechesne CJ, Rabejac D, and Desmadryl G (1994). Development of calretinin immunoreactivity in the mouse inner ear. J. Comp. Neurol 346, 517–529. 10.1002/cne.903460405. [PubMed: 7983242]
35. Dow E, Siletti K, and Hudspeth AJ (2015). Cellular projections from sensory hair cells form polarity-specific scaffolds during synaptogenesis. Genes Dev 29, 1087–1094. 10.1101/gad.259838.115. [PubMed: 25995190]
36. Ding D, Zhang J, Li W, Li D, Yu J, Wu X, Qi W, Liu F, Jiang H, Shi H, et al. (2020). Can auditory brain stem response accurately reflect the cochlear function? J. Neurophysiol 124, 1667–1675. 10.1152/jn.00233.2020. [PubMed: 33026904]
37. Ernfors P, Van De Water T, Loring J, and Jaenisch R (1995). Complementary roles of BDNF and NT-3 in vestibular and auditory development. Neuron 14, 1153–1164. 10.1016/0896-6273(95)90263-5. [PubMed: 7605630]
38. Sun H, Salvi RJ, Ding DL, Hashino DE, Shero M, and Zheng XY (2000). Excitotoxic effect of kainic acid on chicken otoacoustic emissions and cochlear potentials. J. Acoust. Soc. Am 107, 2136–2142. 10.1121/1.428495. [PubMed: 10790039]
39. Xiang M, Maklad A, Pirvola U, and Fritzsch B (2003). Brn3c null mutant mice show long-term, incomplete retention of some afferent inner ear innervation. BMC Neurosci 4, 2. 10.1186/1471-2202-4-2. [PubMed: 12585968]
40. McFadden SL, Ding D, Jiang H, and Salvi RJ (2004). Time course of efferent fiber and spiral ganglion cell degeneration following complete hair cell loss in the chinchilla. Brain Res 997, 40–51. 10.1016/j.brainres.2003.10.031. [PubMed: 14715148]
41. Kersigo J, and Fritzsch B (2015). Inner ear hair cells deteriorate in mice engineered to have no or diminished innervation. Front. Aging Neurosci 7, 33. 10.3389/fnagi.2015.00033. [PubMed: 25852547]
42. Hemond SG, and Morest DK (1992). Tropic effects of otic epithelium on cochleo-vestibular ganglion fiber growth in vitro. Anat. Rec 232, 273–284. 10.1002/ar.1092320212. [PubMed: 1546805]
43. Stevens CB, Davies AL, Battista S, Lewis JH, and Fekete DM (2003). Forced activation of Wnt signaling alters morphogenesis and sensory organ identity in the chicken inner ear. Dev. Biol 261, 149–164. [PubMed: 12941626]

44. Van de Water TR (1988). Tissue interactions and cell differentiation: neurone-sensory cell interaction during otic development. Development 103 (Suppl), 185–193. 10.1242/dev.103.Supplement.185. [PubMed: 3074908]
45. Bianchi LM, and Cohan CS (1993). Effects of the neurotrophins and CNTF on developing statoacoustic neurons: comparison with an otocyst-derived factor. Dev. Biol 159, 353–365. 10.1006/dbio.1993.1247. [PubMed: 8365572]
46. Gu C, Rodriguez ER, Reimert DV, Shu T, Fritzsch B, Richards LJ, Kolodkin AL, and Ginty DD (2003). Neuropilin-1 conveys semaphorin and VEGF signaling during neural and cardiovascular development. Dev. Cell 5, 45–57. 10.1016/s1534-5807(03)00169-2. [PubMed: 12852851]
47. Delacroix L, and Malgrange B (2015). Cochlear afferent innervation development. Hear. Res 330, 157–169. 10.1016/j.heares.2015.07.015. [PubMed: 26231304]
48. Sun S, Babola T, Pregernig G, So KS, Nguyen M, Su SSM, Palermo AT, Bergles DE, Burns JC, and Müller U (2018). Hair Cell Mechanotransduction Regulates Spontaneous Activity and Spiral Ganglion Subtype Specification in the Auditory System. Cell 174, 1247–1263.e15. 10.1016/j.cell.2018.07.008. [PubMed: 30078710]
49. Shrestha BR, Chia C, Wu L, Kujawa SG, Liberman MC, and Goodrich LV (2018). Sensory Neuron Diversity in the Inner Ear Is Shaped by Activity. Cell 174, 1229–1246.e17. 10.1016/j.cell.2018.07.007. [PubMed: 30078709]
50. Pujol R, Pickett SB, Nguyen TB, and Stone JS (2014). Large basolateral processes on type II hair cells are novel processing units in mammalian vestibular organs. J. Comp. Neurol 522, 3141–3159. 10.1002/cne.23625. [PubMed: 24825750]
51. Rehder V, and Kater SB (1992). Regulation of neuronal growth cone filopodia by intracellular calcium. J. Neurosci 12, 3175–3186. 10.1523/JNEUROSCI.12-08-03175.1992. [PubMed: 1494951]
52. Dulon D, Safieddine S, Jones SM, and Petit C (2009). Otoferlin is critical for a highly sensitive and linear calcium-dependent exocytosis at vestibular hair cell ribbon synapses. J. Neurosci 29, 10474–10487. 10.1523/JNEUROSCI.1009-09.2009. [PubMed: 19710301]
53. Pangrsic T, Lasarow L, Reuter K, Takago H, Schwander M, Riedel D, Frank T, Tarantino LM, Bailey JS, Strenzke N, et al. (2010). Hearing requires otoferlin-dependent efficient replenishment of synaptic vesicles in hair cells. Nat. Neurosci 13, 869–876. 10.1038/nn.2578. [PubMed: 20562868]
54. Whitehead MC, and Morest DK (1985). The development of innervation patterns in the avian cochlea. Neuroscience 14, 255–276. 10.1016/0306-4522(85)90177-0. [PubMed: 3974881]
55. Sobkowicz HM, Rose JE, Scott GE, and Slapnick SM (1982). Ribbon synapses in the developing intact and cultured organ of Corti in the mouse. J. Neurosci 2, 942–957. 10.1523/JNEUROSCI.02-07-00942.1982. [PubMed: 7097321]
56. Levic S, Nie L, Tuteja D, Harvey M, Sokolowski BHA, and Yamoah EN (2007). Development and regeneration of hair cells share common functional features. Proc. Natl. Acad. Sci. USA 104, 19108–19113. 10.1073/pnas.0705927104. [PubMed: 18025474]
57. Cotanche DA, Petrell A, and Picard DA (1991). Structural reorganization of hair cells and supporting cells during noise damage, recovery and regeneration in the chick cochlea. Ciba Found. Symp 160, 131–150. 10.1002/9780470514122.ch7. [PubMed: 1752160]
58. Müller M, and Smolders JW (1998). Hair cell regeneration after local application of gentamicin at the round window of the cochlea in the pigeon. Hear. Res 120, 25–36. 10.1016/s0378-5955(98)00049-5. [PubMed: 9667428]
59. Scheibinger M, Janesick A, Diaz GH, and Heller S (2022). Immunohistochemistry and in situ mRNA detection using inner ear vibratome sections. Neuromethods 176, 41–58. 10.1007/978-1-0716-2022-9_3.
60. Ordiway G, McDonnell M, Mohan S, and Sanchez JT (2022). Evaluation of Auditory Brainstem Response in Chicken Hatchlings. J. Vis. Exp 176, e63477. 10.3791/63477.

Highlights

- New auditory hair cells appear 5 days after hair cell loss
- New synapses appear near the basement membrane at the tips of hair cell projections
- Functional recovery starts 11 days after hair cell loss and is complete after 4 weeks
- Cytomorphological maturation time course aligns with recovery of hearing thresholds

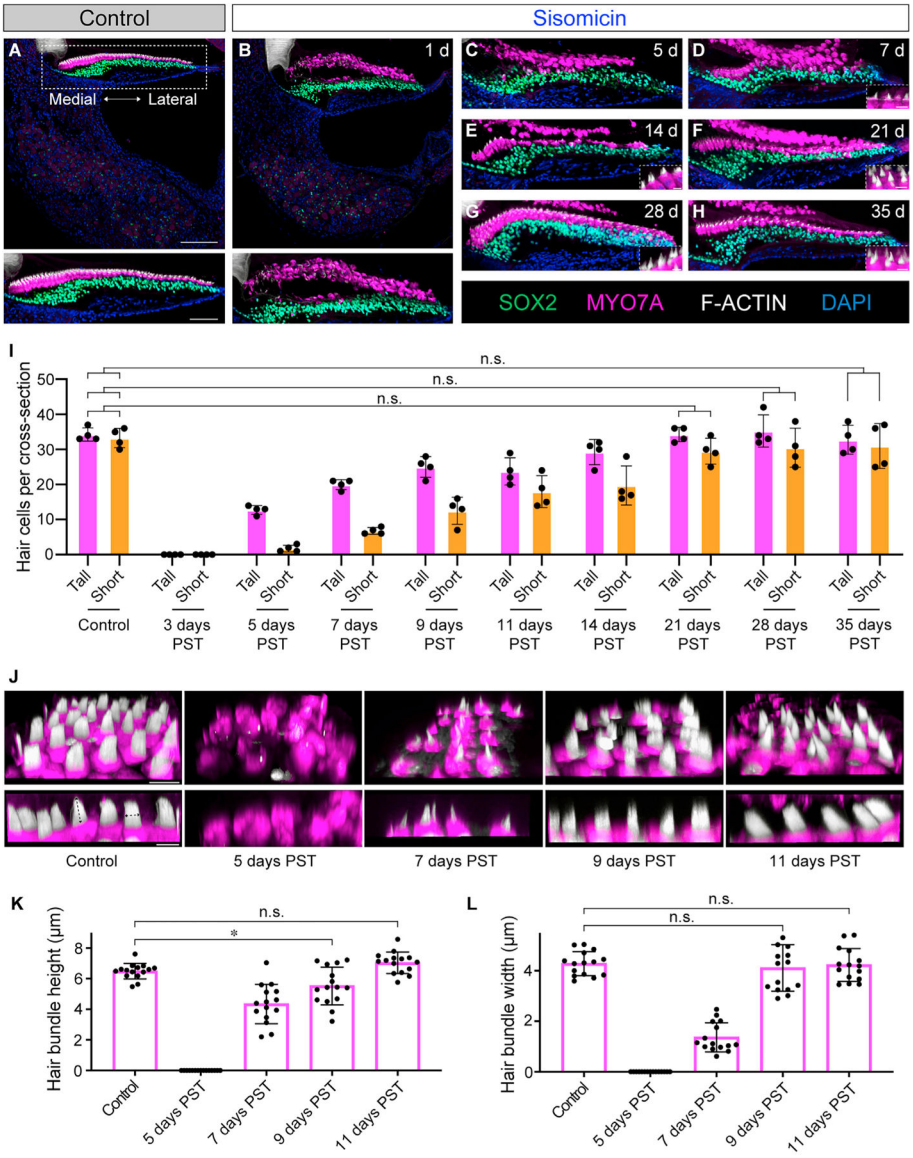

Figure 1. Hair cell regeneration following sisomicin infusion

(A) Transverse vibratome sections through the middle region of the basilar papilla were immunolabeled with antibodies to MYO7A (magenta) to identify hair cells and SOX2 (green) for supporting cells. F-ACTIN in hair bundles was visualized with phalloidin (white). The cell nuclei were stained with DAPI (blue). An enlarged image of the basilar papilla auditory epithelium is shown on the bottom. Tall hair cells are located in the medial region, and short hair cells are located in the lateral region. The medial and lateral regions have also been named neural and abneural, respectively. Scale bars: 100 μm (top) and 50 μm (bottom).

(B–H) All hair cells were extruded into the *scala media* at 1 day PST, and MYO7A-labeled debris was detectable throughout all time points analyzed. Newly regenerated hair cells were first detected 5 days PST; thereafter, the images document how regeneration proceeded up to 21–35 days PST. The insets show hair bundles at different time points. Inset scale bar: 5 μm.

(I) Quantitative analysis of the number of hair cell types per middle region cross-section and single optical section. Means ± SDs are shown. n = 4. The statistical analysis was performed using two-way ANOVA.

(J) Examples of F-actin (white) in hair bundles in control and newly regenerated hair cells in the middle region of the basilar papilla. New hair bundles were detected at 7 days PST and matured over time. The dotted lines in the control indicate how we measured hair bundle height and width. Scale bars: 10 μm (top) and 5 μm (bottom). The top shows oblique side-top views of the specimens, and the bottom provides side views.

(K and L) Quantifications of hair bundle height and width. Means ± SDs are shown. n = 4. The statistical analysis was performed using one-way ANOVA. *$p < 0.05$.

See also Figure S1.

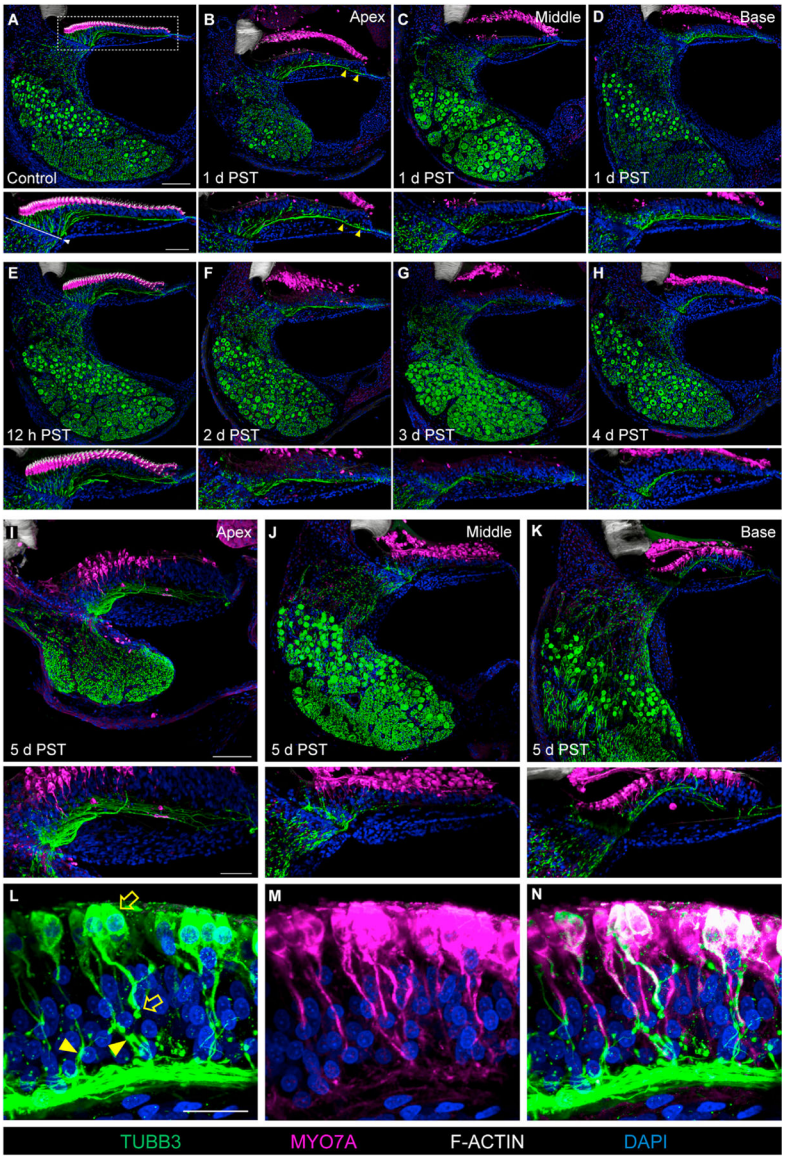

Figure 2. Neurite retraction following hair cell loss

(A) Auditory neurons were visualized with TUBB3 antibody (green). The magnified image representing the dotted box is shown on the bottom. The solid white line indicated by an arrowhead represents the superior fibrocartilaginous plate. Scale bars: 100 μm (top) and 50 μm (bottom).

(B–D) One day PST, the neurites retracted across the basilar papilla shown in sections of distal (apex, B; middle, C; and proximal [base], D) regions. The efferent nerve fibers, highlighted with yellow arrowheads in (B), innervating the hyaline cells, were unaffected.

(E) No changes in neurite morphology were noted at 12 h PST.

(F–H) Neurites retracted progressively after hair cell loss, shown at 2–4 days PST.

(I–K) The neurites regrew when the newly regenerated hair cells emerged based on MYO7A and TUBB3 immunostainings across the basilar papilla. Scale bars: 100 μm (top) and 50 μm (bottom).

(L–N) TUBB3 antibody immunolabeled the newly regenerated hair cells (unfilled arrows) as well as the neurites (filled arrowheads). Scale bar: 20 μm.

See also Figure S2.

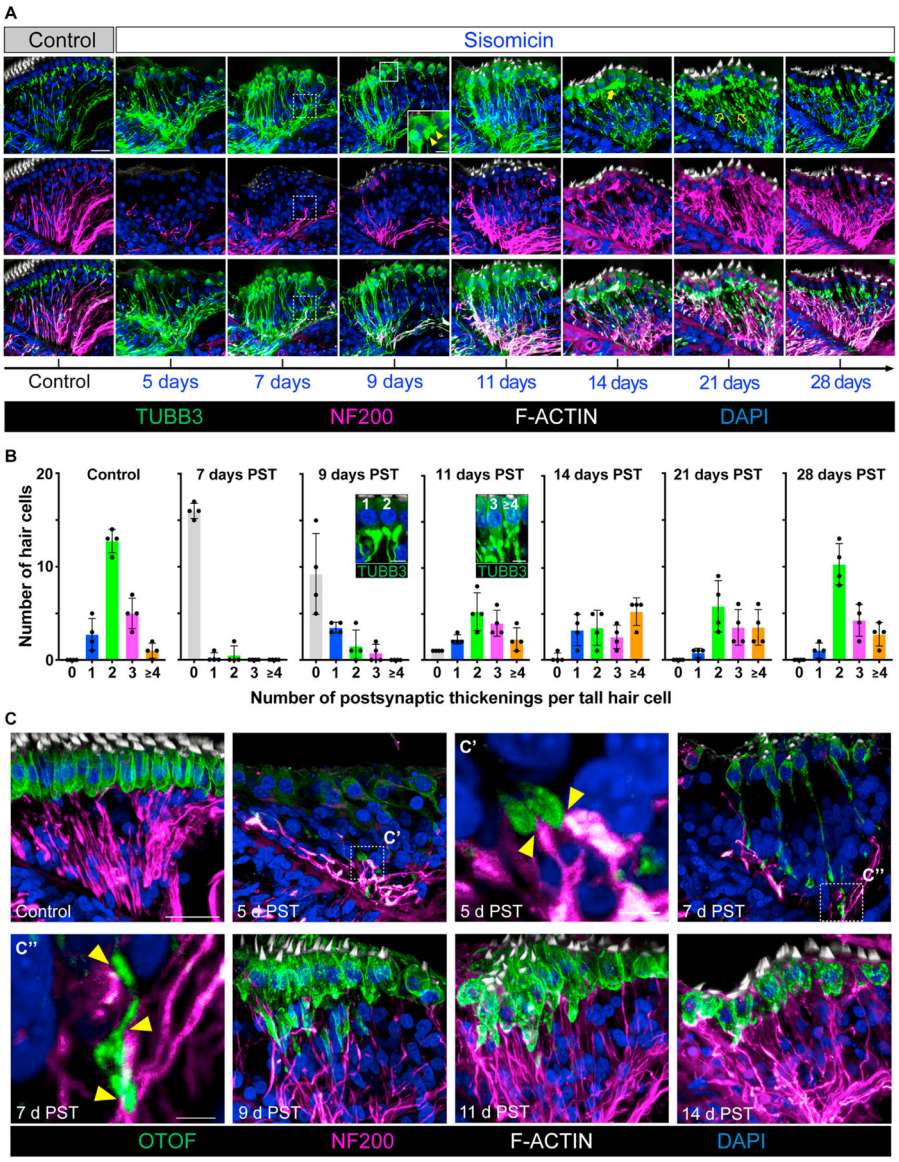

Figure 3. Reinnervation during hair cell regeneration

(A) Cross-sections of medial basilar papilla regions are shown. The control section reveals the normal innervation with TUBB3 (green) and NF200 (magenta) antibodies. At 5–9 days PST, the newly regenerated hair cells display prominent basal protrusions that contact the extending afferent neurites (dotted square). Post-synaptic-like neurite thickenings were first detected at 9 days PST (yellow arrowhead). Large post-synaptic thickenings (filled arrow, 14 days) and neurite buds (unfilled arrows, 21 days) were detectable during reinnervation. Reinnervation appeared complete at 28 days PST. Scale bars: 20 μm and 5 μm for the inset (9 days).

(B) Quantification of post-synaptic-like thickenings during reinnervation. New tall hair cells were categorized into five groups based on the number of post-synaptic thickenings per hair cell. The insets show examples of each group. Scale bar: 5 μm. Means ± SDs are shown. n = 4.

(C) Middle region cross-sections labeled with antibodies to otoferlin (OTOF) and NF200. The tips of hair cell basal projections displayed strong OTOF labeling that appeared in close contact with NF200-positive neurites (yellow arrowheads in C′ and C″). The OTOF-labeled hair cell projections shortened and thickened between PST days 7 and 14. Scale bars: 20 μm and 5 μm.

See also Figures S3 and S4.

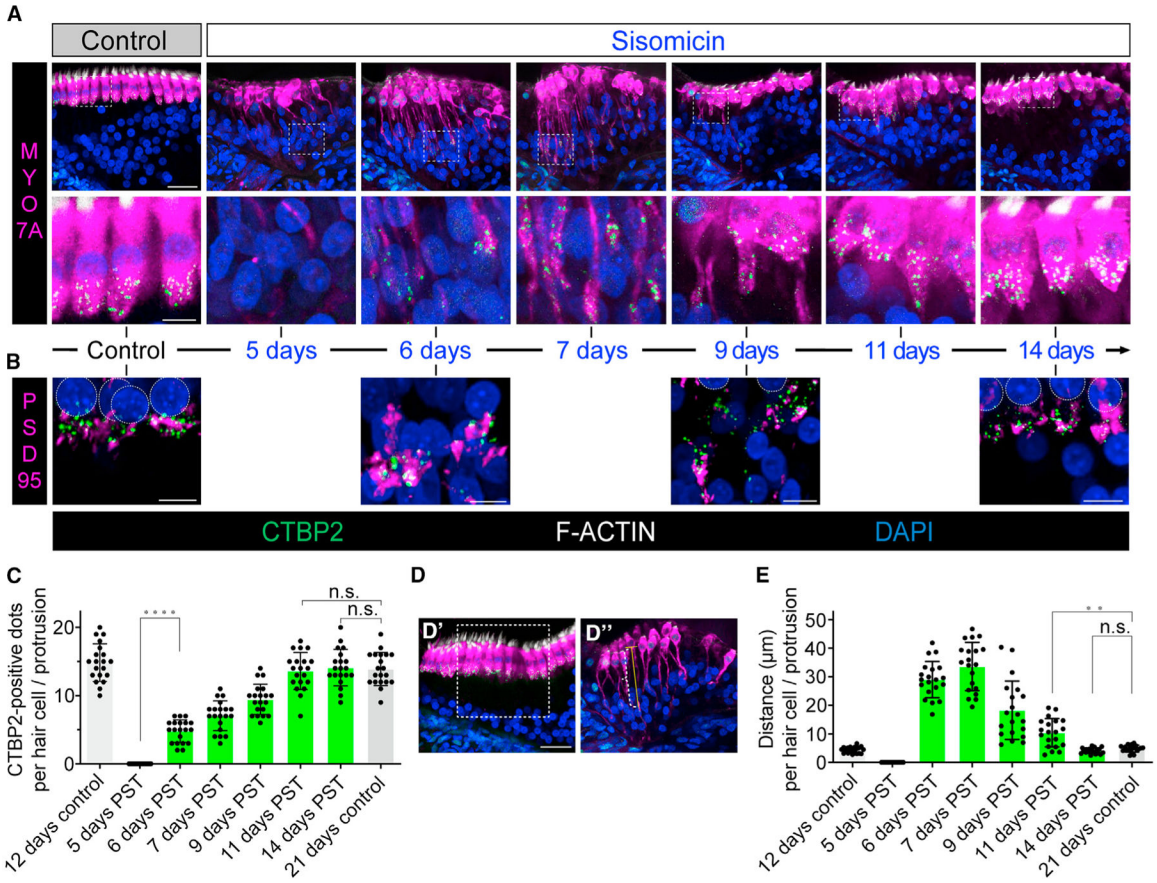

Figure 4. Reappearance of pre- and post-synaptic specializations

(A) CTBP2-positive punctae (green) were detectable below the nuclei of hair cells in medial control sections. New punctae emerged at the tips of the basal protrusion of newly regenerated tall hair cells at 6 days PST and returned to the original position at 14 days PST. Scale bars: 20 µm (top) and 2.5 µm (bottom).

(B) In control tall hair cells, PSD95-positive post-synaptic thickenings (magenta) were associated basolaterally and in proximity to CTBP2-labeled pre-synaptic specializations. From day 6 PST onwards, we observed an association of PSD95-positive neurite tips with CTBP2-positive punctae. We quantified CTBP2-positive punctae associated with individual PSD95-positive thickenings (n = 3; sets of five hair cells per sample) and found 4.7 ± 1.1 CTBP2 punctae per PSD95-labeled structure in controls and 2.2 ± 0.6 per newly regenerated hair cell at 6 days, 2.9 ± 0.9 at 9 days, and 4.5 ± 1.6 after 14 days, on average. The dotted circles label hair cell nuclei. Scale bars: 2.5 µm.

(C and D) Quantification of CTBP2-positive punctae. Data points represent counts for five clearly defined tall hair cells in 60 × 60 × 60 μm^3 volumes (dotted square in D′) and divided by 5 and for individual protrusions that can be traced back to single hair cells. The data are from sections through the middle area of basilar papillae. Means ± SDs are shown. n = 4 independent experiments. Statistical analysis was performed using one-way ANOVA. ****p < 0.0001.

(E)The distance between the nuclei of new hair cells and associated punctae was measured as illustrated in (D″). Means ± SDs are shown. n = 4 independent experiments. Statistical analysis was performed using one-way ANOVA. **p < 0.01. Scale bar: 20 μm.
See also Figure S3.

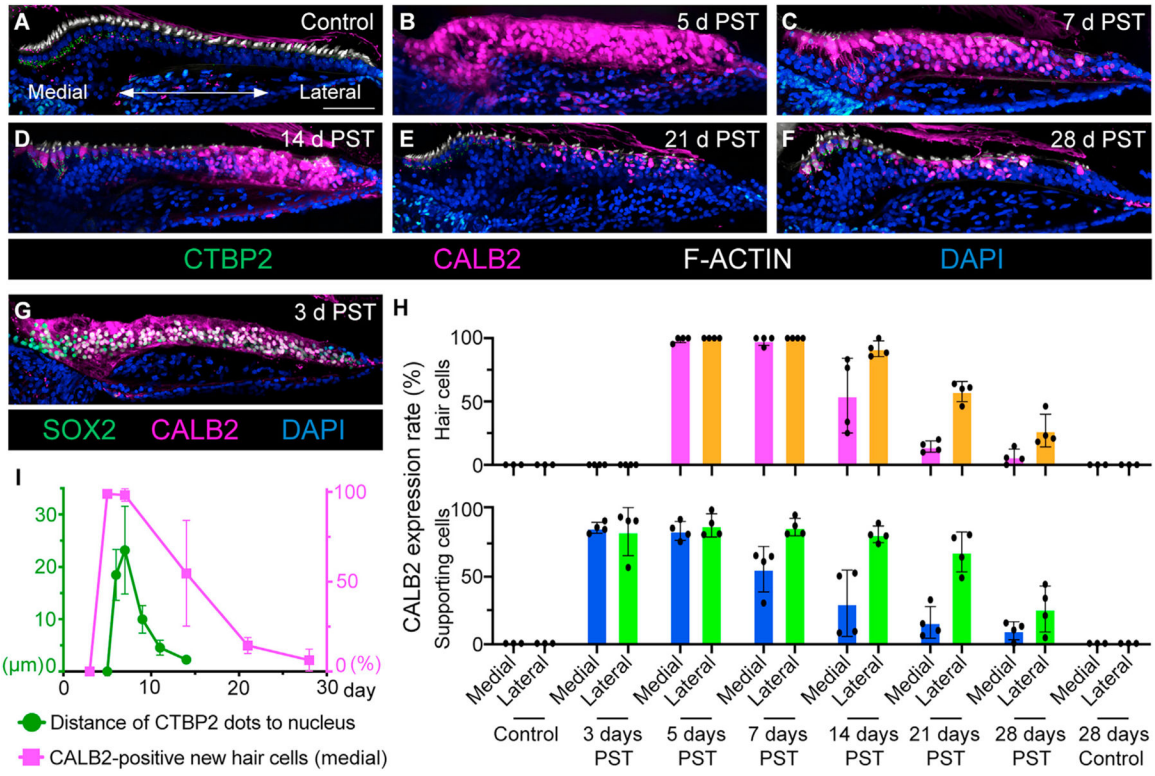

Figure 5. Transition of CALB2 expression during regeneration

(A) In control sections, CALB2/calretinin immunoreactivity (magenta) is absent in mature hair cells and sporadically associated with potential post-synaptic structures. Scale bar: 50 μm.

(B–F) CALB2/calretinin immunoreactivity was detectable in newly regenerated hair cells and in the nuclei of supporting cells. Both distributions gradually shifted toward the lateral side and became sparse 28 days PST.

(G and H) Quantification of CALB2/calretinin expression in regenerated hair cells and the nuclei of supporting cells. (G) shows an example at 3 days PST. White supporting cell nuclei indicate strong double staining with CALB2 and SOX2 antibodies. Medial and lateral sides were divided equally across the basilar papilla. Means ± SDs are shown. n = 3 (control) and 4 (sisomicin-infused group).

(I) Correlation between the distance of CTBP2-positive punctae to the hair cell nucleus and percentile of CALB2-positive new tall hair cells on the medial side. The left y axis indicates the distance, and the right y axis indicates the percentage of CALB2-expressing hair cells. Means ± SDs are shown. n = 4.

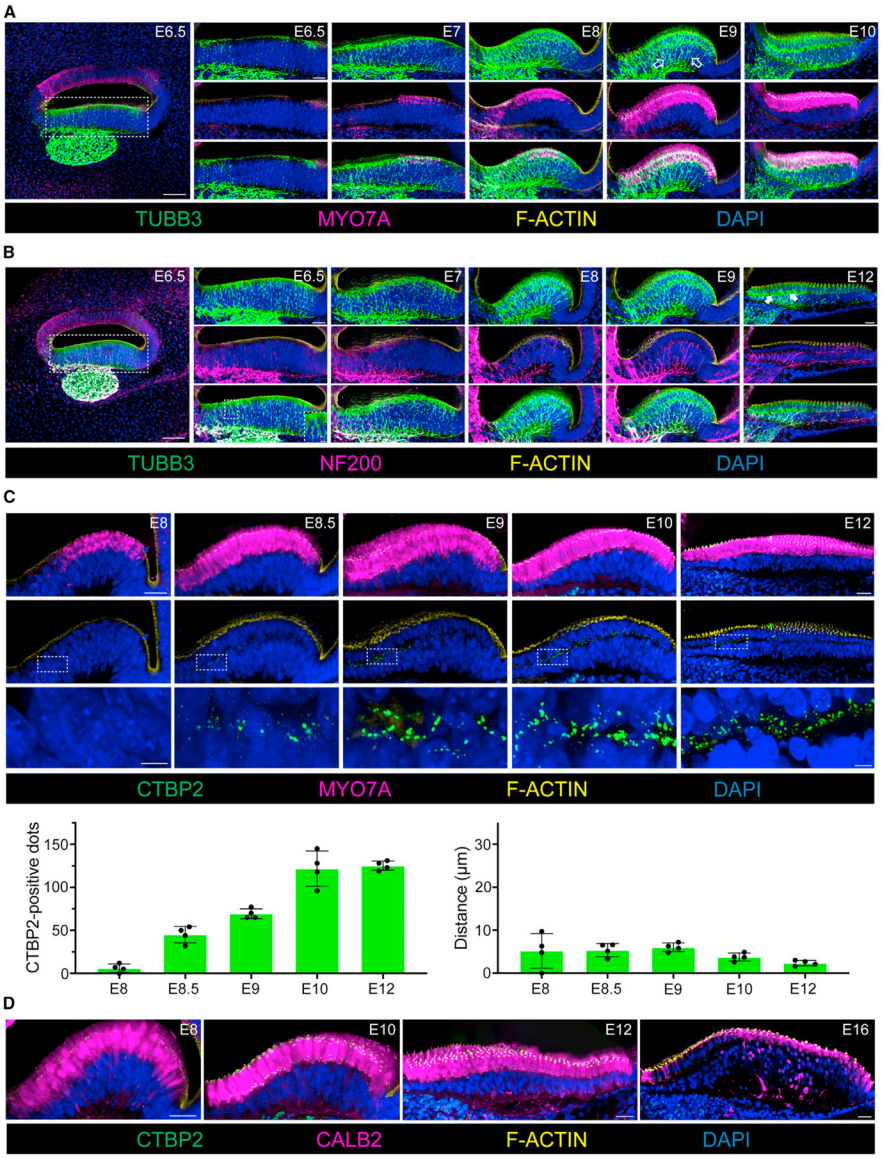

Figure 6. Hair cell differentiation and innervation in embryos

(A and B) Nascent hair cells displaying basal protrusions were detectable as early as E6.5 based on TUBB3 staining. Some NF200-positive neurites extended into the sensory epithelium at E6.5, as indicated by the inset for E6.5, and established post-synaptic-like thickenings with hair cells as early as E8 based on NF200 staining in (B). Neurite buds and post-synaptic thickenings became more frequent at E9 and E12, indicated by white unfilled arrows in A (E9) and filled arrows in B (E12). Scale bars: 50 μm (left), 20 μm (right), and 5 μm (inset).

(C) CTBP2-positive punctae emerged at E8–E8.5. Punctae were counted in consistent 60 μm^2 medial regions, and distances were measured by the same procedure shown in Figure 4. Means ± SDs are shown. n = 4. Scale bars: 20 μm (unmagnified) and 5 μm (magnified).

(D) CALB2/calretinin expression was robustly detected in nascent hair cells and disappeared from the medial side at E16. Scale bar: 20 μm.

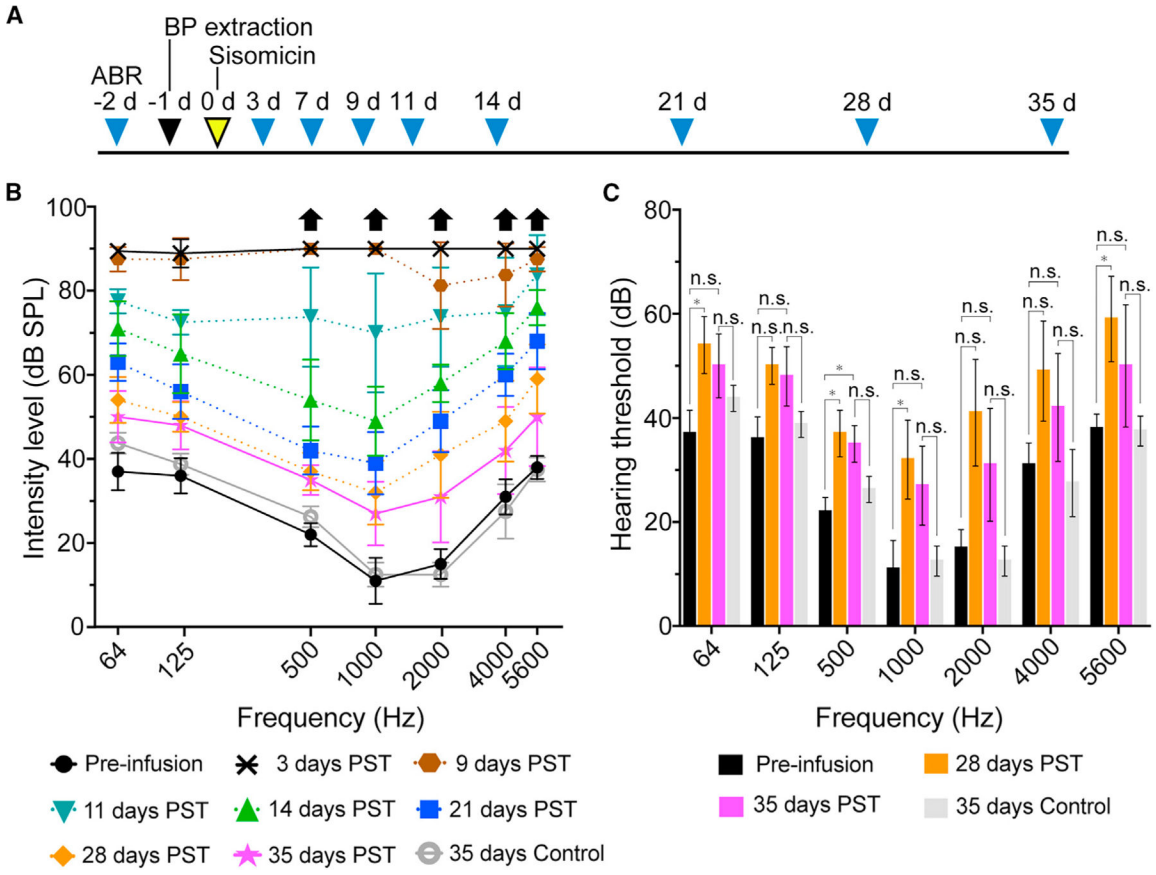

Figure 7. Auditory functional recovery after sisomicin infusion

(A) Time points when ABR measurements were conducted.

(B) Audiogram of ABRs of five chickens observed over time. Hearing began to recover around 9 days PST and returned close to original levels 35 days PST. Means ± SDs are shown. n = 5.

(C) Comparison of 28 days and 35 days PST with pre-infusion and 35 day age-matched controls. Means ± SDs are shown. n = 5. The statistical analysis was performed using Tukey's multiple comparisons test. *p < 0.05.

See also Figure S5.

KEY RESOURCES TABLE

REAGENT or RESOURCE	SOURCE	IDENTIFIER
Antibodies		
Rabbit polyclonal anti-MYOSIN 7A (1:500)	Proteus Biosciences	Cat number 25-6790; RRID:AB_10015251
Mouse monoclonal anti-SOX2-488 (1:200)	Santa Cruz Biotechnology	Cat number sc-365823; RRID:AB_10842165
Rabbit polyclonal anti-Neurofilament 200 (1:800)	Sigma	Cat number N4142-.2ML; RRID:AB_477272
Rabbit polyclonal anti-calretinin (1:1000)	Swant	Cat number 7697; RRID:AB_305702
Rabbit polyclonal anti-PSD95 (1:100)	Invitrogen	Cat number 51-6900
Mouse monoclonal Anti-CTBP2 (1:200)	BD Biosciences	Cat number 612044; RRID:AB_399431
Mouse monoclonal anti-Tubulin β 3 (1:1000)	BioLegend	Cat number 801201
Donkey anti-Rabbit IgG, Alexa Fluor 546 (1:500)	Thermo Fisher Scientific	Cat number A10040; RRID:AB_2534016
Donkey anti-Mouse IgG, Alexa Fluor 488 (1:500)	Thermo Fisher Scientific	Cat number A-21206; RRID:AB_141607
Alexa Fluor 647 Phalloidin (1:50)	Invitrogen	Cat number A22287; RRID:AB_2620155
Chemicals, peptides, and recombinant proteins		
Paraformaldehyde	EMS	Cat number 15710
DAPI (1:5000)	Thermo Fisher Scientific	Cat number D1306; RRID:AB_2629482
Low Melt Agarose	BioRad	Cat number 1613112
Mounting Media (Citifluor CFM-3)	EMS	Cat number 17979-30
Isoflurane, USP	VetOne	Cat number 502017
Carprofen	Millipore Sigma	Cat number SML1713
Sisomicin	Millipore Sigma	Cat number 1612801
Surgical superglue	VetClose, Henry Schein Animal Health	Cat number BS031477
Critical commercial assays		
DeadEnd fluorometric TUNEL System	Promega	Cat number G3250
Experimental models: Organisms/strains		
Fertilized chicken eggs, SPF, Premium	Charles River	10100326
Software and algorithms		
Fiji/ImageJ	Fiji	https://fiji.sc; RRID:SCR_002285
Black Zen	Zeiss	https://www.zeiss.com/microscopy/en_us/products/microscope-software/zen.html; RRID:SCR_018163
Blue Zen	Zeiss	https://www.zeiss.com/microscopy/en_us/products/microscope-software/zen.html; RRID:SCR_013672
GraphPad Prism	Prism_Version 8.4.1	https://www.graphpad.com/scientific-software/prism/
Bitplane Imaris 8.4.1	Oxford Instruments	https://imaris.oxinst.com/